

# Association of Quantum dot nanoparticles with *Pseudomonas aeruginosa* biofilm

Jayne B. Morrow<sup>†</sup>, Catalina Arango P. <sup>‡</sup>, and R. David Holbrook<sup>\*</sup>

<sup>†</sup>Biochemical Science Division, National Institute of Standards and Technology,  
100 Bureau Drive MS 8312, Gaithersburg, MD 20878

<sup>‡</sup>Department of Molecular and Cell Biology Department, University of Connecticut,  
91 N. Eagleville, U-3125, Storrs, CT 06269•

<sup>\*</sup>Surface and Microanalysis Division, National Institute of Standards and Technology,  
100 Bureau Drive MS 8371, Gaithersburg, MD 20878

## Abstract

Quantum dots (QDs) of two different surface chemistries (carboxyl (COOH) and poly ethylene glycol (PEG) modified) were utilized to determine the impact of surface functionality on QD mobility and distribution in *Pseudomonas aeruginosa* PAO1 biofilms. Confocal Laser Scanning Microscopy (CLSM) was utilized to evaluate QD association with biofilm components (proteins, cells and polysaccharides). QDs did not preferentially associate with cell surfaces compared to polysaccharide and protein biofilm matrix materials. Neither PEG nor COOH QDs were found to be internalized by individual bacterial cells. Neither QD functionality nor flowrate of QD application (0.3 or 3.0 ml/min) resulted in a marked difference in QD association with *P. aeruginosa* biofilms. However, center of density determinations indicated COOH QDs could more easily penetrate the biofilm matrix by diffusion than PEG QDs. Biofilms with PEG QDs associated had rougher polysaccharide layers and rougher cell distribution than biofilms with COOH QDs. This work suggests natural biofilms may serve as deposition locations in natural and engineered environmental systems and biofilm structural parameters may change based on exposure to nanomaterials of varied physical characteristics.

## Introduction

Engineered nanoparticles (ENPs) possess many novel chemical, electronic and quantum mechanical properties that make them well suited for numerous applications, including those specific to the microelectronic, automotive, energy, medical, and aerospace industries. Demand for innovation in these industries will be met by an ever-growing number of products containing ENPs, which will also necessitate an increase in production of the raw ENP itself. Such intensification of ENP production and use also

protends an increase of ENP contamination in the natural environment. Indeed, there is already direct evidence of ENP release from consumer products into surface waters (Kaegi, 2008). Consequently, there is a critical need to understand ENP fate and transport in the natural environment, including identification of environmental “sinks” that may tend to promote ENP removal from one phase and subsequent ENP accumulation in another.

One potential environmental “sink” for ENPs in aquatic systems are biofilms. Biofilms are surface-attached communities of microorganisms that predominate at the water/solid surface interfaces and are common to nearly all ecosystems (Costerton et al., 1995). Serving primarily as a survival niche for these microbes (Hall-Stoodley et al., 2004), biofilms are composed of bacterial cells surrounded by extracellular polymeric substances (EPS), which include proteins, DNA and polysaccharides (Sutherland, 2001). EPS components dictate the overall surface chemistry (surface charge and hydrophobicity) of the biofilm (Baoyu Gao, 2008) and play very specific roles in overall biofilm function. For example, protein and divalent metal ions may facilitate biofilm structural changes and stabilize biofilm formation (Baum et al., 2009) while polysaccharides form the scaffolding that provides microcolonies with the ability to disperse and form based on environmental signals (Ma et al., 2009). Furthermore, proteinaceous appendages and motility structures located on individual bacteria are critical to the formation of microcolonies and biofilm maturity and dispersion capabilities (Klausen et al., 2003).

The hypothesis that biofilms may serve as depository for mineral and ENP contaminants appears to be well-supported by reports of colloid-biofilm interactions in

porous media, wastewater reactors, and mineral surfaces (Larsen, 1994; Leon-Morales, 2004; Lo, 1996; Morrow et al., 2005). Interestingly, the majority of studies relating to ENPs to biofilms have focused on the ENP's antimicrobial properties in an effort to reduce biofilm formation (Sambhy, 2006; Weir, 2008) or as a diagnostic tool in probing pathogenic microbial populations within biofilms (Yang et al., 2008). We are aware of only one other study investigating the role of biofilms in ENP removal from the aqueous phase (Ferry, 2009). In that study, 61% of the recovered gold nanorods were found associated with the biofilms; biofilms represented the most important environmental sink in the mesocosm experiments. The ubiquitous nature of biofilms in aquatic systems and their potential for ENP sorption necessitate a better understanding of factors that may improve or hinder ENP-biofilm interactions.

This study examined the distribution of model ENP materials, quantum dots (QDs), in bacterial biofilms as a function of fluid shear and of QD surface chemistry (carboxyl vs. PEG modified). *Pseudomonas aeruginosa* PAO1 biofilms were subjected to pulse carboxyl and PEG modified QD dosing at two flowrates. *Pseudomonas aeruginosa* PAO1 was chosen for this work as it is one of the most studied model biofilm forming organisms with relevance to both clinical and environmental applications. QDs are colloidal semiconductor nanocrystals that are frequently used to model engineered nanomaterials due to their strong photoluminescence and ability for surface functionalization. QD accumulation in the biofilm matrix and biofilm structure were examined using Confocal Laser Scanning Microscopy (CLSM) and differential staining of biofilm components, with the help of the biofilm-analysis software.

## Materials and Methods

**Biofilm growth** *Pseudomonas aeruginosa* PAO1 carrying a constitutive chromosomal green fluorescent protein (GFP) and gentamicin resistance marker (Klausen et al., 2003) was used in all studies. PAO1 liquid cultures and biofilms were grown at 37°C in ABT medium supplemented with sodium citrate (10 mM for liquid medium, 40 mM for plates) (ABTC) (Klausen et al., 2003). Gentamycin (30 µg/ml) was added as necessary.

For biofilm growth, seed cultures were inoculated with a single colony from an ABT plate and grown to late stationary phase ( $OD_{600} = 1.2 \pm 0.2$ ). Cells were harvested by centrifugation (1,500 RPM, 7 minutes) and resuspended in ABTC medium to a final concentration of  $10^7$  cells/ml. The FC 271 flow-cell chamber (1 mm (D) by 10 mm (W) by 50 mm (L); BioSurface Technologies Corp., Bozeman, MT<sup>1</sup>) was first filled with sterile ABTC. One-ml of the cell suspension was added through the sterile inoculation port and cells were allowed to attach to the substrata for 1 hour before flow of ABTC was resumed at a rate of 0.3 or 3.0 ml/min, as indicated. Biofilms accumulated on PVC coupons inside the flow cell were allowed to grow on the PVC surface for 20 hours. All media and experimental components including the flow cell and coupons were sterilized by autoclaving at 121° C, 20 psi for 20 min previous to the experiments.

**Staining of Biofilm Components.** Fluor-conjugated probes used by J. Lawrence et. al. to determine the contribution of specific biofilm constituents including protein, DNA and polysaccharides (Lawrence et al., 2003) were applied here to identify specific biofilm

---

<sup>1</sup> Certain commercial equipment, instruments, or materials are identified in this paper to foster understanding. Such identification does not imply recommendation or endorsement by the National Institute of Standards and Technology, nor does it imply that the materials or equipment identified are necessarily the best available for the purpose.

components (Table 1). Tetramethyl rhodamine isothiocyanate (TRITC)-conjugated *Arachis hypogaea* lectin (PNA) (Sigma-Aldrich, St. Lewis, MO) at 100 µg/ml in phosphate buffered saline (PBS, pH 7.2) solution was used to detect the polysaccharide components of the biofilm, as it binds to galactosyl (β-1,3) N-acetylgalactosamine. Sypro orange (5000x concentrate in DMSO, Invitrogen, Carlsbad, CA), diluted 1/5000 in PBS buffer, was used for differential detection of proteins in the biofilm matrix. Before staining, biofilms were rinsed for 15 minutes with PBS supplied through the input line of the flow cell. The influent was then switched from plain PBS buffer to the Sypro orange solution until the flow cell chamber was filled. The flow was ceased and staining proceeded for 20 minutes, after which the flow cell was rinsed with 10 reactor volumes of PBS to remove any unassociated stain. The biofilm was then stained with TRITC-conjugated PNA lectin in a similar way. Stain solutions were applied with a flow rate of 0.3 ml/min.

**Nanoparticles.** QDs conjugated with two different surface groups were used: COOH (655 ITK, Invitrogen, Hayward, CA) or PEG (Qtracker 655, Invitrogen, Carlsbad, CA). QDs were chosen to represent a range of medically (Gelperina et al., 2005) and environmentally relevant nanomaterials (Lecoanet et al., 2004) in both size and surface charge. The quantum dots were suspended in PBS buffer to a final concentration of 8 pmol/L.

After biofilm components were stained, the influent line was transferred to the QD solution and 10 ml of QDs were continuously added at a constant. The biofilms were rinsed for 10 reactor volumes and all effluent was captured for analysis of QD presence.

QD suspensions were applied through the sterile inoculation port and application fluid flow was resumed at a rate of 0.3 or 3.0 ml/min.

**Electrophoretic Mobility and Effective Diameter Measurements.** Effective diameters and electrophoretic mobility measurements of QD suspensions were obtained via dynamic light scattering measurements using a Zeta PALS Zeta Potential Analyzer (Brookhaven Instruments Corporation, Holtsville, NY). Five measurements with 10 runs per measurement were recorded for each of the QD suspensions.

**Transport Calculations.** The diffusion coefficient was calculated as:

$$D = (k_b T) / (3\pi\eta d_{\text{eff}}) \text{ (m}^2\text{/s)} \quad \text{(Equation 1)}$$

Where  $k_b$  is the Boltzmann's constant ( $1.38065 \times 10^{-23} \text{ m}^2\text{kg/s}^2\text{K}$ ),  $T$  is the temperature in K and  $\eta$  is the liquid viscosity. The diffusion length,  $L_d$ , the characteristic length that a particle could travel based on diffusion alone was calculated as:

$$L_d = \sqrt{4Dt} \text{ (m)} \quad \text{(Equation 2)}$$

where  $t$  is the residence time based on the given flow rate. The Péclet number is a dimensionless ratio of the rate of advection to the rate of diffusion:

$$Pe = (LV)/D \quad \text{(Equation 3)}$$

where  $L$  is the system length,  $V$  is the fluid velocity and  $D$  is the diffusion constant.

**Microscopy and Image Analysis.** Biofilms and QD dissemination were imaged with a Confocal Laser Scanning Microscope (CLMS) (Zeiss LSM 510 Carl Zeiss, MicroImaging, Inc, Thornwood, NY) in triplicate for each condition, locations chosen based on complete randomization. Colocalization coefficients were determined by 3D image reconstruction performed on confocal laser scanning microscopy images of the

biofilm components (channels) as indicated by fluorescent stains. COMSTAT (Heydorn et al., 2000), a computer program for quantitative analysis of biofilms from CLSM image stack was utilized to calculate the total mass ( $\mu\text{m}^3/\mu\text{m}^2$ ), roughness coefficient, surface to volume ratio ( $\mu\text{m}^2/\mu\text{m}^3$ ), average thickness ( $\mu\text{m}$ ), and maximum thickness ( $\mu\text{m}$ ) of the biofilms. The normalized center of density was calculated from COMSTAT-obtained density data for each image in the stack (total area covered by mass), as the first moment of the density with respect to the attachment surface divided by the total density, divided by total density of the stack, normalized to the biofilm thickness.

**Statistical analysis.** Statistical analyses were conducted as follows. To evaluate if the type of QD affected QD distribution in the biofilm, structural parameters obtained from COMSTAT analysis of the QD CLSM data for the two QD types were compared using a single factor ANOVA (regardless of flow regimen) (degrees of freedom = 14). To evaluate if the flow regimen affected either biofilm structure (in one or all of its components) or QD distribution in the biofilm, structural parameters obtained for the two flow regimens from COMSTAT analysis of CLSM data for each component of the biofilm were compared between the two flow regimens, regardless of QD type (degrees of freedom = 12 to 14). For comparison of physical distribution of the different components of the biofilm, a single factor ANOVA was conducted for the three components (cells, proteins, polysaccharides) and QDs. The parameters obtained by COMSTAT analysis of CLSM data for the components were subjected to ANOVA. For p-values below 0.05, confidence intervals for the difference were calculated for each pair of components to identify which ones were significantly different.

For all statistical analyses, a p-value  $\leq 0.05$  was considered indicative of a significant difference, while p-values between 0.05 and 0.1 were not considered statistically significant, but were indicative of a possible effect. p-values above 0.1 were considered as not indicative of a difference. ( $\alpha = 0.05$  for all analysis).

## **Results**

**QD Surface Charge and Hydrodynamic Radius.** The size and surface charge of the QDs in the application medium was determined prior to the deposition experiments to provide insight into the role of nanomaterial physical parameters on deposition behavior. Physical parameters of the QDs are presented in Table 2. Measurements from dynamic light scattering showed that COOH-QDs are slightly smaller than PEG-QDs. Electrophoretic mobility measurements indicate that both QDs have a negative charge, with PEG-QDs being closer to neutrality (Table 2). The diffusion coefficients obtained here were similar to reported values for QDs at 655 spectral emission (Thorne and Nicholson, 2006).

**Image Analysis of Biofilm Components.** Both visual inspection and COMSTAT software were used to analyze the fluorescent signal received for the labeled biofilm matrix materials (Figure 1). CLSM images were obtained using three different channels, with appropriate excitation/emission wavelengths to detect three components in the biofilms represented by different fluorophores: cells (GFP), proteins (Spyro orange stain) and polysaccharides (TRITC-conjugated PNA lectin) described in Table 1. Panel A of Figure 1 indicates a single optical slice in the image stacks analyzed. Panels B and C are 3-D reconstructions of the images from a single stack to provide insight into the

contributions of the components to the overall biofilm. Data from biofilm image stacks obtained from CLSM were pooled for both flow rates and analyzed using the COMSTAT software to calculate total mass, roughness, surface to volume ratio and thickness of each fluorescently labeled biofilm component. Physical features of the biofilms were analyzed to understand the relative contribution of each biofilm component to the overall structure of the biofilm and record any structural differences when contacted with QDs of varied physical characteristics. Values for each parameter of the different biofilm components (cells, protein and polysaccharides) were compared using a single factor ANOVA. Mass measurements (biomass,  $\mu\text{m}^3/\mu\text{m}^2$ ) were higher for biofilm cell components (as determined by the GFP signal in the biofilm) compared to protein and polysaccharide components ( $p = 0.006$ ) indicating a larger proportion of the stained biofilm was GFP labeled cells than the other stained constituents (Table 3). Biomass values for protein labeled components were nearly 20% of the total stained biofilm which is consistent with other reports of PAO1 biofilm component analysis (Sandt et al., 2009).

In addition to biomass, other physical attributes can be examined to understand the impact of QD association to the biofilm matrix materials. The roughness coefficient, an indicator of heterogeneity or thickness variation for a given analyte, was lower for GFP cells ( $p = 0.05$ ) than stained proteins and the polysaccharides. A notable increase in biofilm heterogeneity was observed for both cells and polysaccharides in biofilms exposed to PEG QDs compared to COOH QDs (Table 3). Since the surface to biovolume ratio is an indicator of the recorded void space for that biofilm component, not necessarily a physical void in the biofilm matrix, it is an additional measure of

heterogeneity for biofilm components. Surface to biovolume ratios were notably higher for both cell and polysaccharide components in biofilms contacted with PEG QDs.

The impact of the flow rate on biofilm constituents was determined by analyzing the individual structural features calculated for data collected under the different flow rates. The only structural features found to be significantly impacted by flow rate were the roughness coefficient and normalized center of density for the cell fraction of the biofilm (Table 3). The high-flow regimen yielded larger heterogeneity in the cell distribution and a higher center of density than the lower flow rate.

**QD Association with Biofilm Matrix Materials.** Both visual inspection and COMSTAT software was used to analyze the fluorescent signal received for the given QDs once associated with the biofilm matrix materials. Visual inspection of CLS microscopy images revealed clear QD association with stained *P. aeruginosa* biofilms (Figure 1). CLSM images suggest both COOH and PEG QDs associated with and were able to penetrate the biofilm regardless of surface functionality. However, QDs were never directly associated with the substratum surface in the combined excitation/emission images and were rarely observed on the biofilm surfaces, directly adjacent to the bulk liquid.

COMSTAT image analysis software was utilized to determine QD functionality impacts on the structural distribution parameters for QDs. The data was pooled to determine statistically significant differences in structural values among the images. Surface to volume ratios for the COOH QDs were larger than for the PEG QDs ( $p = 0.017$ ) (Table 4). As was stated for the cell and polysaccharide components of the

biofilm, a larger surface to volume ratio is an indicator of greater heterogeneity in the component under analysis and not necessarily an indication of void space as the void volume may be filled with another biofilm component. The normalized center of density values was higher for the PEG QDs than the COOH QDs. Additionally, a ten fold increase in flow rate had no impact on QD/biofilm association parameters (Table 4).

In order to determine if QDs had a higher affinity for a specific biofilm component, overlap coefficients were calculated for QD signals with biofilm component signals (Table 5). QD-protein overlap coefficients were higher than QD-cell and QD-polysaccharide coefficients regardless of applied flow rate and QD type.

## **Discussion**

### **Nanoparticle Transport and Deposition in Biofilm**

Particle association and deposition with the biofilm matrix materials is a function of the transport mechanisms and surface association potential due to particle and biofilm surface chemistry. Both biofilm structure and particle size have been shown to contribute to deviations in particle diffusion from Brownian behavior (Guiot et al., 2002). In the study conducted here, it is important to note that QD contact with the biofilm is expected to occur through a simple depletion transport model in a plug flow reactor. Transport due to simple depletion was determined by calculating the Péclet number,  $Pe$ , a dimensionless number that defines the relationship between the rate of advection and the rate of diffusion for particles in a given flow regime. Due to the large Péclet numbers calculated at each of the flow rates, convection is the dominant transport mechanism over the length of the chamber but diffusion dominates penetration into the biofilm in the

vertical dimension. Differences in calculated diffusion coefficients and diffusion length for the QDs evaluated provide insight into the observed differences in the normalized center of density for both the COOH and PEG QDs. The normalized center of density for the COOH QDs is closer to the substratum surface than for PEG QDs which is consistent with the shorter diffusion lengths calculated for PEG QDs. Although diffusion of the particles in the biofilm is believed to be governed by the particle size, the role of QD functionalization on biofilm penetration cannot be completely separated from particle size in this study. The slightly smaller, negatively charged COOH QDs were able to more effectively penetrate the biofilms where the normalized center of density was farther from the substratum for the larger, near neutral PEG QDs. Consistent with our observations, Guiot et. al. observed free diffusion of anionic, COOH functionalized particles up to 110 nm in diameter in low EPS producing *L. lactis* biofilms and for particles up to 28 nm in thick EPS biofilms of *S. maltophilia* and a near complete inhibition of association for positively charged amine-modified latex beads (Guiot 2002).

Two different flow rates were examined to determine if increased fluid shear as a function of convective transport would impact the accumulation of nanomaterials in the biofilm or the biofilm structure. The high-flow regimen yielded larger heterogeneity in the cell distribution and a higher center of density for biofilm components than the lower flow rate. Fluid shear is known to contribute to structural differences in biofilms (Stoodley et al., 2002a; Stoodley et al., 2002b). Biofilm structures have been recorded to elongate under increased shear and higher shear resulted in more rigid and stronger *P. aeruginosa* biofilms (Stoodley et al., 1999). Although differences were noted in biofilm

structure due to the higher flow rates, there were no significant impacts on QD association and penetration into the biofilm matrix due to flow rate.

The only significant difference observed in the QD association parameters due to the QD functionalization was in surface to volume ratio (Table 4). However, the larger surfaces to volume ratios calculated by COMSTAT for COOH QDs compared to PEG QDs are directly related to the smaller diameter of the COOH QDs. The PEG QDs were 1.4 times as large as the COOH QDs resulting in a smaller surface to volume ratio of individual QDs identical in proportion to the surface to volume ratio difference calculated for QDs associated with the biofilm.

### **Nanoparticle Association with Biofilm Matrix Materials**

Once in proximity of the biofilm, observed differences in QD association with the biofilm matrix materials included higher overlap coefficients with protein matrix components. Upon introduction of QD ENPs to the biofilm system, enhanced association was expected due to known differences in surface chemistry for biofilm components (Baoyu Gao, 2008). However, the role of constituent biofilm matrix materials in QD association had not been previously measured. Observed values for overlap coefficients were higher for proteins than other biofilm components for both QDs (Table 5) suggesting a higher QD affinity for the protein fraction of the biofilm. The greater association to proteins may be a result of ion-ion or dipole induced interactions between QD surface groups and proteins harbored in the biofilm matrix. Protein interaction with PEG polymers has been long studied as a means of protein separation (Atha and Ingham, 1981). Proteins readily associate with carboxylate functional groups on nanoparticles (Worrall et al., 2006) and COOH groups are critical for protein binding in engineered

nanoparticles with protective monolayers (You et al., 2005). Additionally, staining of the proteins is not believed to contribute to QD association as Sypro orange fluorescent labeling of proteins results in non-covalent interaction between the dye and the folded protein (Newman et al., 2002). Isoelectric values for the Sypro orange-protein complexes have been found to remain unchanged compared to unassociated proteins (Newman et al., 2002) suggesting surface charge interactions are still possible even on dye-bound protein surfaces.

The observation of a greater QD ENPs association with protein components of the biofilm may aid in both nanomaterial manufacturing waste stream treatment procedures as well as predictive models for environmental transport. Some biofilms used to purify waste streams produce protein to polysaccharide ratios of 2/1 depending on the bacterial species and location in the filter (Baoyu Gao, 2008). ENP deposition and removal may be enhanced with higher protein to polysaccharide ratios as those found in biofilters and waste stream treatment processes can be designed to utilize this removal mechanism. ENP deposition in biofilms native to aquatic ecosystems can lead to exposure through the food web (Ferry, 2009). Aquatic organisms, such as tetrahymena, capable of grazing on bacterial biofilms have been shown to accumulate the same QDs used in this study (Holbrook et al., 2008). This work suggests that ENP transport and deposition in environmental systems may be largely influenced by biofilm accumulation and biofilms are logical sinks to examine when monitoring ENP accumulation in environmental ecosystems.

Finally, some interesting differences in structural parameters for labeled biofilm components were observed when contacted with the two different QD materials. The

roughness coefficient, an indicator of heterogeneity or thickness variation for a given analyte, was lower for GFP cells ( $p = 0.05$ ) than for stained proteins and the polysaccharides. Uniformity in cell distribution is consistent morphology for relatively young biofilms (Stoodley et al., 2002a) as were generated in this study. As biofilms mature and become more diverse, heterogeneity in biofilm components increases as does the distribution of cells and cell phenotypes. Statistically larger roughness coefficients for biofilm components (cells and polysaccharides) exposed to PEG QDs is an indication of QD impact on biofilm structure possibly due to an increase in physico-chemical interactions due to the PEG coated QDs. PEG is a nontoxic, water-soluble synthetic polymer that has been shown to promote the hybridization of cells (Vaughan et al., 1976) and precipitate proteins (Atha and Ingham, 1981). Increasing cell-cell interaction may disrupt some of the native ion-ion and dipole interactions of the biofilm matrix resulting in a destabilization and increase in structural heterogeneity. However, consistent with our previous results (Holbrook et al., 2008), co-localization analysis indicated that internal labeling of GFP cells did not occur. Internal labeling has only been shown for some gram-negative and gram-positive strains for small QDs ( $< 5$  nm) (Kloepfer et al., 2005).

## **Conclusions**

Observations of PEG and COOH QDs, model ENPs, deposition and association with a bacterial biofilm provides insight into the role of nanomaterial characteristics on their fate and transport. This work concludes demonstrates the utility in accounting for the interaction of ENPs with proteins and other components in biofilm systems, to enhance our understanding of nanomaterial deposition in native biofilms and potentially

enhance our ability to engineer advanced waste stream treatment processes. As nanomaterials become increasingly functionalized for surface activity it will be increasingly important to develop methods to remove them from the waste streams of manufacturing facilities and for water treatment purposes. In the case of the ENPs studied here, enhancing the ratio of protein to polysaccharide by utilizing different bacterial species may increase deposition and alter deposition location. Biofilms are known reservoirs for particles in the environment and this work further indicates the potential role of biofilms in fate and transport of ENPs in environmental systems.

### **Acknowledgement**

*Pseudomonas aeruginosa* PAO1 cultures were kindly provided by Dr. Tim Tolker-Nielsen and Dr. Mikkel Klausen of the Technical University of Denmark, Lyngby, Denmark.

### **References**

- Atha D.H., Ingham K.C. (1981) Mechanism of Precipitation of Proteins by Polyethylene Glycols. *The Journal of Biological Chemistry* 256:12108-12117.
- Baoyu Gao X.Z.C.X.Q.Y.W.L.J.W. (2008) Influence of extracellular polymeric substances on microbial activity and cell hydrophobicity in biofilms. *Journal of Chemical Technology & Biotechnology* 83:227-232.
- Baum M., Kainovic A., O'Keeffe T., Pandita R., McDonald K., Wu S., Webster P. (2009) Characterization of structures in biofilms formed by a *Pseudomonas fluorescens* isolated from soil. *BMC Microbiology* 9:103.
- Costerton J.W., Lewandowski Z., Caldwell D.E., Korber D.R., Lappin-Scott H.M. (1995) Microbial biofilms. *Annual Reviews Microbiology* 49:711-745.
- Ferry J.L.C., P.; Hexel, C.; Sisco, P.; Frey, R.; Pennington, P.L.; Fulton, M.H.; Scott, I.G.; Decho, A.W.; Kashiwada, S.; Murphy, C.J.; Shaw, T.J. . (2009) Transfer of Gold Nanoparticles From the Water Column to the Estuarine Food Web. *Nature Nanotechnology* 4:441-444

- Gelperina S., Kisich K., Iseman M.D., Heifets L. (2005) The Potential Advantages of Nanoparticle Drug Delivery Systems in Chemotherapy of Tuberculosis. *Am. J. Respir. Crit. Care Med.* 172:1487-1490. DOI: 10.1164/rccm.200504-613PP.
- Guiot E., Georges P., Brun A., Fontaine-Aupart M.P., Bellon-Fontaine M.-N., Briandet R. (2002) Heterogeneity of Diffusion Inside Microbial Biofilms Determined by Fluorescence Correlation Spectroscopy Under Two-photon Excitation. *Photochemistry and Photobiology* 75:570-578.
- Hall-Stoodley L., Costerton J.W., Stoodley P. (2004) Bacterial biofilms: from the natural environment to infectious disease. *National Reviews in Microbiology* 2:95-108.
- Heydorn A., Nielsen A.T., Hentzer M., Sternberg C., Givskov M., Ersboll B.K., Molin S. (2000) Quantification of biofilm structures by the novel computer program COMSTAT. *Microbiology* 146:2395-2407.
- Holbrook R.D., Murphy K.E., Morrow J.B., Cole K.D. (2008) Trophic transfer of nanoparticles in a simplified invertebrate food web. *Nature Nanotechnology* 3:352-355.
- Kaegi R.U., A.; Sinnet, B.; Vonbank, R.; Wichser, A.; Zuleeg, S.; Simmler, H.; Brunner, S.; Vonmont, H.; Burkhardt, M.; Boller, M. (2008) Synthetic TiO<sub>2</sub> Nanoparticle Emission From Exterior Facades Into the Aquatic Environment. *Environmental Pollution* 156:233-239.
- Klausen M., Heydorn A., Ragas A., Lambertsen L., Aaes-Jørgensen A., Molin S., Tolker-Nielsen T. (2003) Biofilm formation by *Pseudomonas aeruginosa* wildtype, flagella, and type IV pili mutants. *Molecular Microbiology* 48:1511-1524.
- Kloepfer J.A., Mielke R.E., Nadeau J.L. (2005) Uptake of CdSe and CdSe/ZnS Quantum Dots into Bacteria via Purine-dependent Mechanisms. *Applied and Environmental Microbiology* 71:2548-2557.
- Larsen T.A.H., P. . (1994) Degradation Mechanisms of Colloidal Organic-Matter in Biofilm Reactors. *Water Research* 28:1443-1452.
- Lawrence J.R., Swerhone G.D.W., Leppard G.G., Araki T., Zhang X., West M.M., Hitchcock A.P. (2003) Scanning Transmission X-Ray, Laser Scanning, and Transmission Electron Microscopy Mapping of the Exopolymeric Matrix of Microbial Biofilms. *Appl. Environ. Microbiol.* 69:5543-5554. DOI: 10.1128/aem.69.9.5543-5554.2003.
- Lecoanet H.F., Bottero J.-Y., Wiesner M.R. (2004) Laboratory Assessment of the Mobility of Nanomaterials in Porous Media. *Environmental Science & Technology* 38:5164-5169.
- Leon-Morales C.F.L., A.P.; Strathmann, M.; Flemming, H.C. (2004) Interactions Between Laponite and Microbial Biofilms in Porous Media: Implications for Colloid Transport and Biofilm Stability. *Water Research* 38:3614-3626.
- Lo W.H.N., Y.M.; Lion, L.W.; Shuler, M.L.; Ghiorse, W.C. (1996) Determination of Iron Colloid Size Distribution in the Presence of Suspended Cells: Application to Iron Deposition Onto a Biofilm Surface. *Water Research* 30:2413-2423.
- Ma L., Conover M., Lu H., Parsek M.R., Bayles K., Wozniak D.J. (2009) Assembly and Development of the *Pseudomonas aeruginosa* Biofilm Matrix. *PLoS Pathog* 5:e1000354.
- Morrow J.B., Stratton R.S., Yang H.-H., Smets B.F., Grasso D. (2005) Macro- and Nanoscale Observations of Adhesive Behavior for Several *E. coli* Strains

- (O157:H7 and Environmental Isolates) on Mineral Surfaces. *Environmental Science & Technology* 39:6395-6404.
- Newman S.K.S., Tiemin H., Janusz P. (2002) Laser-induced fluorescence detection of non-covalently labeled protein in capillary isoelectric focusing. *Journal of Separation Science* 25:1119-1122.
- Sambhy V.M., M.M.; Peterson, B.R.; Sen, A. (2006) Silver Bromide Nanoparticle/Polymer Composites: Dual Action Tunable Antimicrobial Materials. *Journal of the American Chemical Society* 128:9798-9808.
- Sandt C., Smith-Palmer T., Comeau J., Pink D. (2009) Quantification of water and biomass in small colony variant PAO1 biofilms by confocal Raman microspectroscopy. *Applied Microbiology and Biotechnology* 83:1171-1182.
- Stoodley P., Lewandowski Z., Boyle D.J., Lappin-Scott H.M. (1999) Structural deformations of bacterial biofilms caused by short-term fluctuations in fluid shear: an in situ investigation of biofilm rheology. *Biotechnology and Bioengineering* 65:83-92.
- Stoodley P., Sauer K., Davies D.G., Costerton J.W. (2002a) Biofilms as Complex Differentiated Communities. *Annu Rev Microbiol* 56:187 - 209.
- Stoodley P., Cargo R., Rupp C.J., Wilson S., Klapper I. (2002b) Biofilm material properties as related to shear-induced deformation and detachment phenomena. *Journal of Industrial Microbiology and Biotechnology* 29:361-367.
- Sutherland I.W. (2001) The biofilm matrix - an immobilized but dynamic microbial environment. *Trends in Microbiology* 9:222-227.
- Thorne R.G., Nicholson C. (2006) In vivo diffusion analysis with quantum dots and dextrans predicts the width of brain extracellular space. *PNAS* 103:5567-5572.
- Vaughan V.L., Hansen D., Stadler J. (1976) Parameters of polyethylene glycol-induced cell fusion and hybridization in lymphoid cell lines *Somatic Cell and Molecular Genetics* 2:537-544.
- Weir E.L., A.; Whelan, A.; Regan, F. (2008) The Use of Nanoparticles in Anti-Microbial Materials and Their Characterization. *Analyst* 133:835-845.
- Worrall J.W.E., Verma A., Yan H., Rotello V.M. (2006) "Cleaning" of nanoparticle inhibitors via proteolysis of adsorbed proteins. *Chemical Communications*:2338-2340.
- Yang H.-H., Morrow J.B., Grasso D., Vinopal R., Deschesne A., Smets B.F. (2008) Antecedent Growth Conditions Alter Retention of Environmental *Escherichia coli* Isolates in Transiently Wetted Porous Media. *Environmental Science & Technology* 42:9310-9316.
- You C.-C., De M., Rotello V.M. (2005) Monolayer-protected nanoparticle-protein interactions. *Current Opinion in Chemical Biology* 9:639-646.

**Table 1. Fluorescent and fluor-conjugated probes applied in this study**

Probe	Ex/Em (nm)	Target
COOH Quantum dot	488/655	nonspecific
PEG Quantum dot	488/655	nonspecific
SyproOrange	470/570	Protein
TRITC conjugated PNA	554/576	$\beta$ -Gal(1-3)galNAc

**Table 2. Experimental Parameters at QD Association**

Parameter	Value
Flow rate,	
	Q <sub>1</sub> 0.3 ml/min
	Q <sub>2</sub> 3.0 ml/min
Flow cell volume	0.5 ml
Temperature	22 ± 1 °C
pH	7.2
Ionic Strength (PBS)	0.150 M
Nanoparticle electrophoretic mobility,	
	COOH QD -1.48 ± 0.24 m <sup>2</sup> /Vs
	PEG QD -0.12 ± 0.68 m <sup>2</sup> /Vs
Nanoparticle effective diameter,	
	COOH QD 23 ± 8 nm
	PEG QD 32 ± 9 nm
Diffusion coefficient,	
	COOH QD 2.13 x 10 <sup>-11</sup> m <sup>2</sup> /s <sup>b</sup>
	PEG QD 1.53 x 10 <sup>-11</sup> m <sup>2</sup> /s <sup>b</sup>
Péclet Number <sup>c</sup> ,	
	Pe <sub>1</sub> 173
	Pe <sub>2</sub> 1739
Diffusion length,	
	L <sub>d1</sub> COOH 2.9 x 10 <sup>-6</sup> m
	L <sub>d2</sub> COOH 2.5 x 10 <sup>-6</sup> m
	L <sub>d1</sub> PEG 0.9 x 10 <sup>-6</sup> m
	L <sub>d2</sub> PEG 0.8 x 10 <sup>-6</sup> m

<sup>a</sup>Suspensions polydispersity values close to zero indicate a monodisperse suspension.

<sup>b</sup>Diffusion coefficients are consistent with reported values for QDs with 655 emission (Thorne and Nicholson, 2006)

<sup>c</sup>Peclet numbers were calculated for low flow rate (subscript 1) and high flow rate (subscript 2).

**Table 3. Parameters of physical properties and distribution of biofilm components, obtained from COMSTAT analysis**

Proteins	Quantum dot type			Flow rate (ml/min)		
	COOH	PEG	p-value	0.3	3.0	p-value
Total Biomass ( $\mu\text{m}^3/\mu\text{m}^2$ )	12.42 (11.54)	12.50 (9.43)	0.99	14.33 (11.10)	9.10 (8.05)	0.38
Roughness coefficient (dimensionless <sup>g</sup> )	0.59 (0.91)	0.22 (0.4)	0.34	0.55 (0.85)	0.14 (0.11)	0.31
Surface to biovolume ratio ( $\mu\text{m}^2/\mu\text{m}^3$ )	2.60 (2.21)	1.62 (0.91)	0.31	2.32 (2.11)	1.77 (0.48)	0.55
Average thickness ( $\mu\text{m}$ )	17.36 (13.07)	20.50 (6.88)	0.58	19.35 (12.34)	20.09 (6.82)	0.91
Maximum thickness ( $\mu\text{m}$ )	23.87 (5.5)	28.07 (7.32)	0.25	25.29 (6.45)	27.20 (7.42)	0.96
Normalized center of Density (dimensionless <sup>h</sup> )	0.46 (0.04)	0.47 (0.05)	0.52	0.46 (0.04)	0.47 (0.06)	0.87
Cells	Quantum dot type			Flow rate (ml/min)		
	COOH	PEG	p-value	0.3	3.0	p-value
Total Biomass ( $\mu\text{m}^3/\mu\text{m}^2$ )	21.54 (3.74)	22.81 (4.37)	0.56	22.00 (4.02)	22.63 (4.39)	0.79
Roughness coefficient (dimensionless <sup>g</sup> )	<b>0.007 (0.002)<sup>a</sup></b>	<b>0.012 (0.005)<sup>a</sup></b>	<b>0.02</b>	<b>0.008 (0.004)<sup>f</sup></b>	<b>0.012 (0.004)<sup>f</sup></b>	<b>0.07</b>
Surface to biovolume ratio ( $\mu\text{m}^2/\mu\text{m}^3$ )	<b>0.79 (0.25)<sup>e</sup></b>	<b>1.15 (0.45)<sup>e</sup></b>	<b>0.09</b>	1.05 (0.43)	0.83 (0.32)	0.33
Average thickness ( $\mu\text{m}$ )	24.49 (4.69)	28.93 (7.36)	0.19	26.83 (6.45)	26.91 (7.26)	0.98
Maximum thickness ( $\mu\text{m}$ )	24.59 (4.71)	29.92 (7.55)	0.18	27.01 (6.61)	27.2 (7.42)	0.96
Normalized center of Density (dimensionless <sup>h</sup> )	0.48 (0.01)	0.49 (0.02)	0.13	<b>0.48 (0.01)<sup>b</sup></b>	<b>0.49 (0.01)<sup>b</sup></b>	<b>0.05</b>
Polysaccharide	Quantum dot type			Flow rate (ml/min)		
	COOH	PEG	p-value	0.3	3.0	p-value
Total Biomass ( $\mu\text{m}^3/\mu\text{m}^2$ )	14.91 (2.72)	13.64 (2.06)	0.56	14.33 (2.74)	14.03 (1.76)	0.83
Roughness coefficient (dimensionless <sup>g</sup> )	<b>0.014 (0.01)<sup>c</sup></b>	<b>0.063 (0.04)<sup>c</sup></b>	<b>0.01</b>	0.036 (0.04)	0.049 (0.04)	0.57
Surface to biovolume ratio ( $\mu\text{m}^2/\mu\text{m}^3$ )	<b>0.61 (0.15)<sup>d</sup></b>	<b>0.78 (0.13)<sup>d</sup></b>	<b>0.04</b>	0.69 (0.16)	0.72 (0.18)	0.69
Average thickness	24.29 (4.45)	25.99 (5.7)	0.54	25.31 (5.11)	24.98 (5.53)	0.91

( $\mu\text{m}$ )						
Maximum thickness	24.59 (4.71)	29.25 (7.55)	0.18	27.01 (6.61)	27.2 (7.42)	0.96
( $\mu\text{m}$ )						
Normalized center of Density (dimensionless <sup>h</sup> )	0.33 (0.04)	0.38 (0.08)	0.16	0.35 (0.07)	0.37 (0.06)	0.57

Average values (one standard deviation)  
<sup>a,b,c,d</sup>: **Difference is statistically significant**  
<sup>e,f</sup>: difference is notarious but not statistically significant  
<sup>g</sup>: Range: zero to infinity  
<sup>h</sup>: Range: zero to one

**Table 4. Parameters of QD distribution in *P. aeruginosa* biofilms, obtained from COMSTAT analysis.**

	Quantum dot type			Flow rate (ml/min)		
	COOH	PEG	p-value	0.3	3.0	p-value
Total mass ( $\mu\text{m}^3/\mu\text{m}^2$ )	7.93 (4.77)	9.18 (4.62)	0.62	9.19 (4.63)	7.42 (4.70)	0.50
Roughness coefficient (dimensionless <sup>c</sup> )	0.072 (0.04)	0.089 (0.06)	0.56	0.073 (0.06)	0.096 (0.04)	0.44
Surface to volume ratio ( $\mu\text{m}^2/\mu\text{m}^3$ )	<b>2.49 (0.51)<sup>a</sup></b>	<b>1.93 (0.26)<sup>a</sup></b>	0.017	2.23 (0.56)	2.12 (0.69)	0.69
Average thickness ( $\mu\text{m}$ )	21.87 (5.69)	22.89 (3.85)	0.69	22.92 (4.66)	21.30 (4.98)	0.57
Maximum thickness ( $\mu\text{m}$ )	24.59 (4.71)	29.25 (7.55)	0.18	27.01 (6.61)	27.20 (7.42)	0.96
Normalized center of Density (dimensionless <sup>d</sup> )	<b>0.38 (0.07)<sup>b</sup></b>	<b>0.46 (0.08)<sup>b</sup></b>	<b>0.07</b>	0.41 (0.09)	0.44 (0.08)	0.47

Average values (one standard deviation)  
<sup>a</sup>: difference is statistically significant  
<sup>b</sup>: difference is notarious but not statistically significant  
<sup>c</sup>: Range: zero to infinity  
<sup>d</sup>: Range: zero to one

**Table 5. Overlap Coefficient Summary.**

	Low Flow Rate (0.3 ml/min)		High Flow rate (3.0 ml/min)	
	COOH	PEG	COOH	PEG
Cells	0.52 (0.05)	0.69 (0.01)	0.62 (0.09)	0.64 (0.06)
Protein	0.65 (0.06)*	0.74 (0.03)*	0.72 (0.07)*	0.79 (0.02)*
Polysaccharide	0.53 (0.12)	0.66 (0.01)	0.64 (0.04)	0.59 (0.09)

Average values (one standard deviation)

\* indicates statistically larger than for cells or polysaccharide components ( $p \leq 0.09$ ).

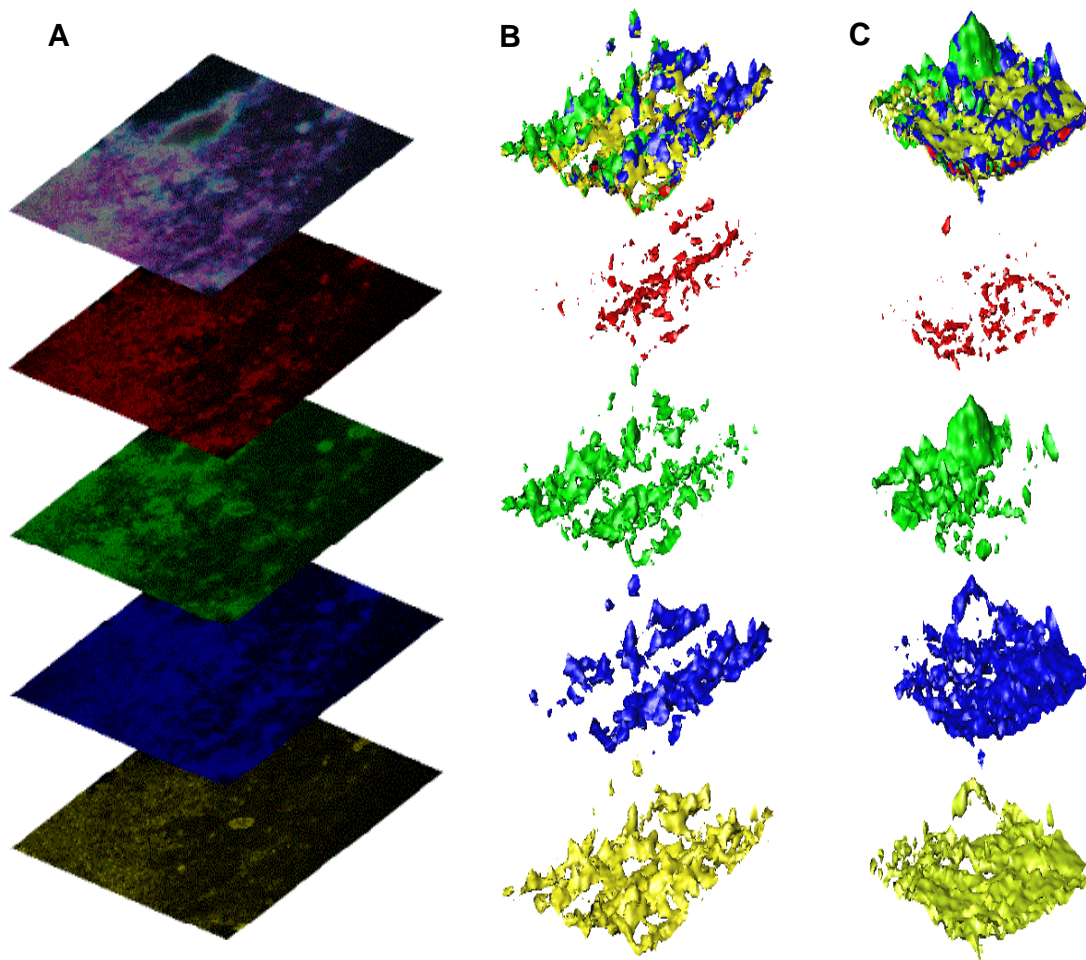


**Figure 1. CLSM images and 3D reconstruction of *P. aeruginosa* PAO1 biofilm samples.** (A) Single optical slice ( $230\ \mu\text{m} \times 230\ \mu\text{m}$ ) from stack containing 79 images at  $0.5\ \mu\text{m}$  section thickness. From top to bottom, slices include composite, QD (shown in false red, collected at 488/635 LP), GFP (false green, 488/505-530 BP), Sypro Orange (false blue, 488/560-615 BP), and TRITC PNA lectin (false yellow, 543/530 – 600 BP). (B) 3-D reconstruction of image stack showing fluorophore surfaces and COOH QD distribution. (C) 3D reconstruction of image stack showing fluorophore surfaces and PEG QD distribution. Colors and fluorophore order of surfaces in (B) and (C) are identical to those listed in (A).